Pressure distributions on modern asymmetric spinnakers

Trans RINA, Vol 152, Part B1, Intl J Small Craft Tech, 2010 Jan-Jun

PRESSURE DISTRIBUTIONS ON MODERN ASYMMETRIC SPINNAKERS

I M Viola, R G J Flay, Yacht Research Unit, Mechanical Engineering Department, The University of Auckland, New Zealand

SUMMARY

An electronically scanned multi-channel pressure system was used at the Yacht Research Unit's Twisted Flow Wind Tunnel (University of Auckland) to test 3 asymmetric spinnakers. The sails were designed for the most recent America's Cup Rule (AC33) and tested on a large-scale model. The present paper focuses on pressure measurements on three asymmetric spinnakers, which were measured on 5 chord-wise sections with 11 pressure taps on each section. All the 3 sails were tested at apparent wind angles of 40°, 55° and 70° and at heel angles of 0°, 10° and 20°. The 3 sails were firstly tested in uniform flow and then one of the sails was re-tested in twisted flow conditions. It was found that the suction peak on the A2 sail increased when the model was heeled to 10°, and then decreased when the heel angle was increased further to 20°, which agrees with the similar observed behaviour in the drive force variation with heel angle. Measurements in straight and twisted flow showed that all sail's secions gave higher suctions in the twisted flow and a corresponding increase in the drive force.

NOMENCLATURE

AC	America's Cup
AC33	33rd America's Cup Class (2nd hypoth.)
AC90	33rd America's Cup Class (1st hypoth.)
AWA	Apparent wind angle (deg)
CFD	Computational fluid dynamics
Cp	Pressure coefficient (-)
Cx	Drive force coefficient (-)
DOG	Deed of Gift
h	Model height
IACC	International America's Cup Class
Mid-section	Horizontal section of the sails at 1/2 of the mitre height
Mitre	Line made up of the points on the sail surface equally far from the leech and the luff
q	Dynamic pressure coefficient (Pa)
SA	Sail area (m^2)
YRU	Yacht Research Unit
z	Vertical height (m)

1. INTRODUCTION

In a previous paper by the same authors [1], aerodynamic forces and the pressure measurements on large-scale models tested in the Yacht Research Unit's Twisted Flow Wind Tunnel at the University of Auckland were presented. In particular, 3 asymmetric spinnakers coupled with the same mainsail were measured at 3 apparent wind angles and 3 heel angles. The force measurements were used to correlate the aerodynamic forces with the optimum sailing condition of each sail. The general pressure distribution measured on the asymmetrics was also presented and correlated with the flow field around the sail. The present work describes in detail the pressure measurements recorded at the same time as the force measurements. They show how the pressure distribution changes when there are changes in boat heel, apparent wind angle, sail shape, and finally, due to testing in uniform flow and twisted flow.

In the previous paper [1], a brief review of downwind sail wind tunnel measurements was presented, noting the increasing interest in asymmetric spinnakers. In particular, the evolution of the America's Cup and Volvo Ocean Race class rules reflects the increasing desire to sail with asymmetric spinnakers tacked onto bowsprits instead of symmetric spinnakers tacked onto poles.

:mentary review to [1], in the ıollowing section the state of the art of pressure measurements on sails is presented, both at full-scale and through wind-tunnel experiments.

2. STATE OF THE ART

Warner and Ober measured pressure distributions on a mainsail and jib in 1923 as reported by Marchaj [2]. Manometers were used to measure 28 points on the leeward side of the sails of the yacht *Papoose* in a full-scale experiment. Since then, for many years there is no knowledge of pressure measurements on sails from the published literature. Half a century later, in the 1970s, Gentry was interested in the slot effect due to the jib/mainsail interaction and investigated their pressure distributions with an Analogue Field Plotter on a 2D model [3]. He was involved in the design of the masts for the America's Cup (AC) defenders *Courageous, Freedom* and *Liberty* in the 1974 and 1977, 1980, 1983 AC defences respectively [4]. These were investigated with the Computational Fluid Dynamic (CFD) code of the Boeing Commercial Airplane Company. In the 1980s, Wilkinson studied the mast-sail interaction on a 2D model-scale section during his PhD [5] and also in successive research [6], [7]. After these few authors, pressure measurements on sails have rarely been published.

Thanks to the authors above, CFD codes were tuned and validated, for instance [8], which allowed a deeper understanding of the pressure distribution and, very importantly, the correlation of the pressure with the velocity field. However, the complexity of the aerodynamics of the sail presents a significant challenge to most current CFD codes. The thin profile can easily lead to a leading edge laminar separation that is followed by transition and turbulent reattachment [9], [10]. In addition, the high curvature causes a strong adverse pressure gradient, which leads to separation [11]. Transition, reattachment and separation, which don't occur around surfaces with sharp curvatures, are still a challenge for CFD codes. Two-dimensional high grid-resolution simulations have been successfully performed matching experimental data, for instance [12], but the computational effort does not allow computations to be performed with the same grid accuracy for a complex 3D geometry. Moreover, the more we understand about sail aerodynamics, the more questionable it appears to be to model the sails in 2D.

In the last 3 years, full-scale measurements have made a resurgence and new lightweight, small devices have allowed better measurements to be taken. The Yacht Research Unit (YRU) at the University of Auckland is developing a wireless pressure system for full-scale experiments to overcome the problems associated with using the wired pressure system developed in 2006 for full-scale sail testing [13]. Similar systems were also developed by an Italian research team [14] and by an American team collaborating with the AC challenger BMW Oracle Racing [15].

At the current state of the art, these systems have provided pressure measurements at only a few points and haven't yet been able to provide a complete pressure map on the sails. They have been used on upwind sails where the rigidity of sails allows the weight of the devices to be carried, and the stability of the sail leads to a more reliable measurement. In the near future, full-scale pressure measurements will hopefully allow complete pressure maps of both upwind and downwind sails.

Finally, in the past year at the YRU's wind tunnel, double-surface rigid sails with pressure tubes inside were tested and the pressure distributions on both the windward and leeward sides of a fully 3D symmetrical spinnaker were measured [16]. The pressure was measured with 8 pressure taps at each of 7 horizontal sections of a 1/25th model-scale International America's Cup Class (IACC) spinnaker sailing at an apparent wind angle (AWA) of 120°.

The experiment presented in this paper was performed with the aim of improving the accuracy of the previous experiment [16] by increasing the model-scale from 1/25th to 1/15th, which led to a larger model, and also by increasing the dynamic pressure from 4.7Pa to 7.5Pa.

Two new class rules were developed for potential use in the 33rd AC: the AC90 and the AC33 classes. Although it appears at the present time that the format of the 33rd AC will be a "Dead of Gift" (DOG) match in multi-hulls, significant design work has been conducted on the AC90 and AC33 classes.
Both of these rules would lead to much faster boats than the previous IACC design. They were to have long bowsprits and to sail with asymmetric spinnakers only. Hence the new tests had the aim of investigating the more recent downwind sails designed for the AC33 rule and the closer AWAs which would be sailed by these faster designs than the former IACC rule which they were to replace.

3. YRU EXPERIMENTS

3.1 TEST CONFIGURATIONS

Three asymmetric spinnakers were tested with the same mainsail. The sails had different shapes and sail areas. In fact, as for an airfoil, a flatter sail performs better at smaller angles of attack, while a more cambered sail performs better at larger angle of attacks. The angle of attack of a sail section (the angle between the wind direction and the chord of the sail section) increases with the AWA (the angle between the wind direction and the boat heading). Hence, a flatter sail performs better at smaller AWAs and a more cambered sail performs better at larger AWAs. In a windward-leeward course as the AC course is, to reach the lower mark in the shortest time, a yacht sails at smaller AWAs in light wind and at larger AWAs with more breeze. Hence, in light wind conditions a flatter sail has to be flown. In very light conditions, a large spinnaker might be too heavy to fly and hence, a smaller sail area (*SA*) is desirable. The three asymmetric spinnakers tested were labelled A1, A2 and A3, respectively. The A1 had the smallest *SA* and flat sections and was designed for light wind and small AWAs; the A2 had an intermediate *SA* and was a general purpose sail; the A3 had the largest *SA* and deep sections and was designed for stronger winds and larger AWAs. The main dimensions are summarised in [1]. Each sail was tested in 5 configurations: at 40°, 55°, 70° AWA with 10° heel; and at 0°, 10°, 20° heel with 55° AWA. Conventional cloth sails were used so as to be able to trim the sail for the maximum drive force. For each condition, two spinnaker sheeting trims were considered: the trim maximising the drive force which can lead the luff to flap in some cases, and a tighter trim required to stabilise the luff and stop it flapping. In the present paper only the trims corresponding to a stable luff are considered.

The tests were performed in uniform flow (without twisting vanes) but all of the configurations measured with the A3 were re-measured with the twisted flow to investigate how the twisted flow changed the pressure distribution on the spinnaker. The reference wind speed

was roughly 3.5m/s giving a Reynolds number based on the model height h equal to $6 \cdot 10^5$. This is less than the full-scale Re by a factor of about 20. In uniform flow, the turbulence intensity was lower than 3%.

The bare-hull model was stiff enough to avoid any deformations while the rigging allowed a similar mast bend to that one achieved in full-scale. The sailcloth used for the sails was the same as used in full-scale but with a properly scaled thickness. This allowed the model-scale sails to stretch and fly as in full-scale.

3.2 PRESSURE MEASUREMENT SYSTEM AND PRESSURE TAP LOCATIONS

A pressure system capable of acquiring up to 512 channels simultaneously, made up of 8 64-channel modules, was used for the investigation. Only 2 of the 8 modules were used. The differential transducers are temperature-compensated *Honeywell XSCL04D* and were used for every channel. The 2 modules were placed in the model cockpit. Miniature lightweight plastic pressure taps 20mm long, 10mm wide and 4mm height were made and attached with double-sided tape to the sail on the opposite side to that under investigation. A 1 mm diameter hole was made in the sail to allow pressure transmission to the tap, resulting in no modification of the local pressure coefficient due to the pressure tap itself. Pressure taps were placed on 5 horizontal sections at heights of 1/8, 1/4, 1/2, 3/4 and 7/8 of the mitre (line made up of the points on the sail surface equally far from the leech and the luff). Eleven pressure taps were located on each section: at 1/12, 1/6, 1/4, 3/8, 1/2, 5/8, 3/4, 5/6, 11/12 of the curve length, plus one as close as possible to the luff and one as close as possible to the leech. To minimise the number of tubes on the model that could affect the aerodynamics, the pressure distributions were measured on one sail surface at a time, hence 5x11=55 pressure measurements were recorded simultaneously.

Fifty-five tubes connected the pressure taps to the modules (Figure 1). To minimise the effect of the tubes on the flow field, the tubes connected to the top two sections of the spinnaker were fed through the head of the mast and then along the windward side shrouds to the modules on the cockpit; the tubes connected to the forward half of the bottom sections were horizontally suspended to the mast and then collected with the upper tubes on the windward shrouds; the tubes connected to the aft half of the bottom sections came to the cockpit along the spinnaker sheet. The pressure tubes of the 2 top sections were 3.2m in length and the other tubes were 2.4m long. The internal diameter of the tubes was 1.5mm. The length of the tubes did not allow high frequency pressure fluctuations to be measured. Hence a relatively low sampling rate of 100Hz was used to minimise the post-processing computational time. Pressures were recorded and averaged over a 70s acquisition period.

Figure 1: the AC33 1/15th scale model set up for tests.

All the transducers were pneumatically connected to a reference static pressure measured with a Pitot-static probe located approximately 10m upstream at the topmast height. Five other Pitot-static probes at different locations were used to correct the reference static pressure although the pressure differences were small enough to be neglected. The total pressure from the reference Pitot-static probe was connected to an additional transducer, which measured the reference dynamic pressure q (roughly 7.5Pa). The pressure differences from each channel were divided by q to provide the pressure coefficients Cp.
More than one transducer measured the dynamic reference pressure and the average value was used.

3.3 FORCES AND MOMENTS MEASUREMENT SYSTEM

The model was fixed to a 6-component balance via 3 brackets and the hull was partially immersed in a pool of water to act as an airtight seal between the hull and the wind tunnel floor. The forces and moments measured by the balance were transformed into non-dimensional coefficients by dividing the forces by the product of q and SA, and by dividing the moments by the product of q, SA and the height of the model h (2.3m). Forces and moments were acquired for 70s at 200Hz.

3.4 INFLOW CONDITIONS

The YRU's Twisted Flow Wind Tunnel has a special vane device to twist the flow upstream of the model test section (Figure 1) [17], which has been recently enhanced after the investigation performed in [18] and which can also be removed from the test section to enable testing in uniform flow. All the tests reported in this paper were performed in uniform flow except for the additional configurations measured with the A3 which were also re-tested with twisted flow to investigate how the twisted flow changes the pressure distribution on the spinnaker.

In uniform flow, the turbulence intensity was less than 3% (while in twisted flow the average turbulence intensity cannot be defined precisely because it varies horizontally due to the presence of the wakes from the vanes). Both in uniform and twisted flow conditions the boundary layer was confined to the lowest 10% of the height of the model.

4. RESULTS & DISCUSSION

The pressure distribution on the asymmetric spinnakers changes in each tested condition but a general trend can be described. Figure 2 shows the pressure coefficient trend on the 5 sections measured. The pressure coefficient on the windward side remains roughly constant, equal to one, for most of the curve length and then decreases to match the negative windward pressure coefficient at the trailing edge. The pressure coefficient on the leeward side shows a first suction peak followed by a pressure recovery, which is correlated to the leading edge separation and reattachment. Then a second suction peak occurs due to the sail curvature. The adverse pressure gradient of the following pressure recovery leads to trailing edge separation, which is evident from the constant negative value of the pressure coefficient. The flow is fully separated on the highest sections and, after a high suction peak at the leading edge, the pressure recovery is almost linear. On the lowest sections the trailing edge separation occurs generally before that on the mid-section.

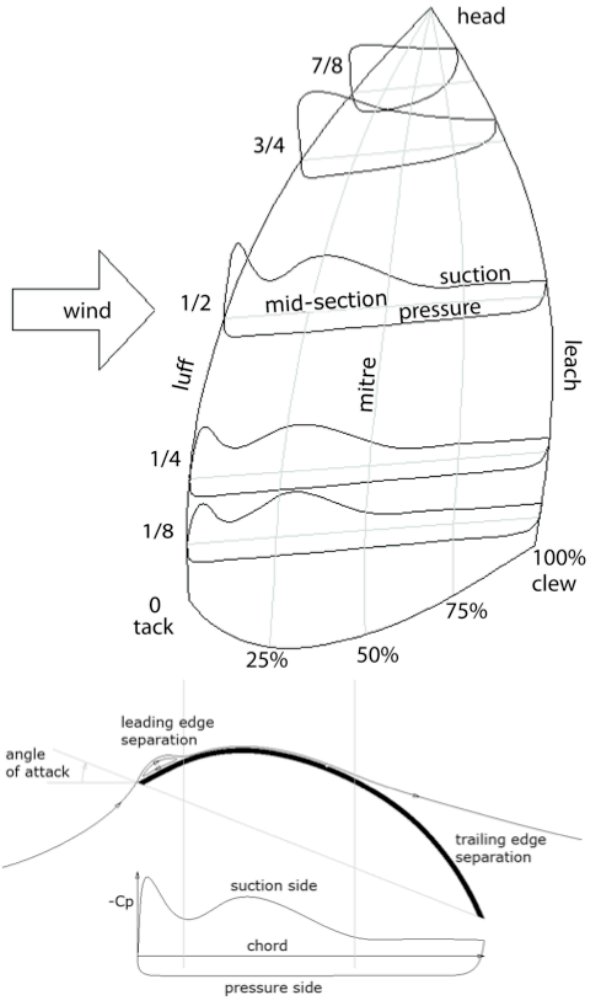

Figure 2: Schematic diagram of the pressure distribution over the asymmetric spinnakers at 5 horizontal heights and the corresponding flow field.

In the following, section 4.1 shows the effect of increasing AWA on the general pressure trends described above. At each AWA the sail was re-trimmed to achieve the maximum drive force leading to a different geometry and a different angle between the wind and the boat model. Section 4.2 shows the effect of increasing the heel angle. When the heel angle is increased, the geometry of the sail remains roughly unchanged and only rotates around the longitudinal boat axis, which leads to a geometrical reduction of the angle between the wind and the sail geometry. Section 4.3 shows the differences between the pressure distributions on the three sail shapes. Finally, section 4.4 shows the effect of testing in twisted flow on the pressure distribution.

4.1 EFFECT OF AWA

When the AWA was increased, the sail's sheet was eased to maximise the drive force and, consequently, the geometry of the sail changed significantly. However, despite the sheet easing, the angle of attack between the reference wind direction and the sail (measured, for instance, between the wind direction and the chord between the tack and the clew) also increased. Figure 3 shows 3 photographs of the A1 at 10° heel from a camera on the roof of the wind tunnel. It can be clearly seen that even if the spinnaker sheet is eased, the angle of attack increases and the camber of the foot becomes larger. The increase in angle of attack causes the separated region to enlarge. Moreover, by easing the sheet the camber of the sail increases, which leads to a larger pressure suction. The adverse pressure gradient after a larger suction peak can eventually lead to a larger trailing edge separation. In brief, increasing the AWA leads to a larger suction peak until an excessive separation occurs at the trailing edge.

Easing the sheet results in the direction of the resultant aerodynamic force turning forward in the direction of the drive force component. This effect is stronger than any reduction in the pressure forces due to an earlier separation. Hence the drive force always increases with the AWA in the range being investigated.

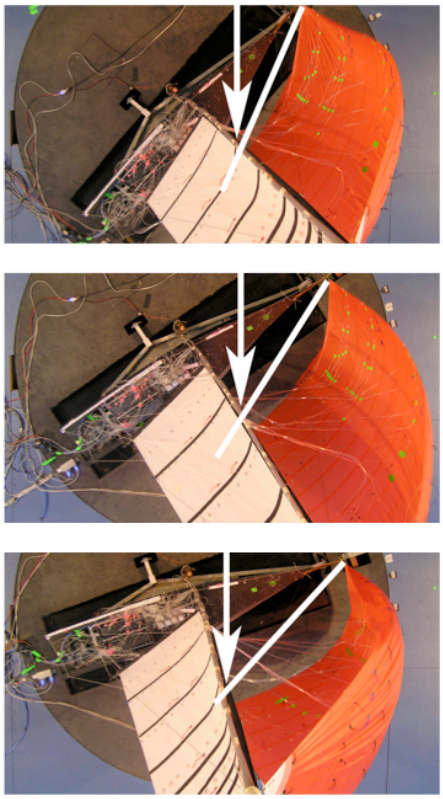

Figure 3: The A1 is photographed from above at 40° (top), 55° (middle), 70° (bottom) AWA. The arrow shows the wind direction and the line shows the chord measured at the sail foot.

Figure 4 shows the pressure coefficients of the 5 measured horizontal sections of the A2 at 10° heel, at 7/8, 3/4, 1/2, 1/4, and 1/8 of the mitre, respectively. At each section, the Cp's measured at 40°, 55° and 70° AWA are compared. On the top section, at 7/8 of the mitre, the pressure trend shows a fully separated flow at each AWA. At the ½ mid-section and at the lower sections, the pressure trends show a reattachment in the first 10% of the curve length and a successive suction peak, followed by a trailing edge separation at 60%-70% of the curve length. The second suction peak increases when the AWA increases from 40° to 55° because of the increased camber. Then it decreases because the trailing edge separation points moves forward to 30%-50% of the curve length. Increasing the AWA and thus the angle of attack, causes the leading-edge suction peak to increase but it does not significantly change the location of the reattachment point.

4.2 EFFECT OF HEEL

In downwind sailing, inducing the boat to heel can cause the aerodynamic forces to increase. The reason why this happens is still not completely understood and future investigation will be required. This work shows that the force increase is mainly due to the increased suction on the leeward side of the spinnaker. Figure 5 shows the pressure distribution along the curve length measured on the 5 horizontal sections of the A2 sailing at 55° AWA. Force measurements show that the drive force increases when the heel is increased from 0° to 10°, and then significantly decreases when heeled further. Figure 5 shows that heeling the model from 0° to 10° causes the suction pressure to increase and then heeling the model further to 20°, causes the suction to decrease due to the trailing edge separation point moving forward.

Some possible interpretations that should be investigated in future research are now discussed. It can be assumed that:

i. The pressure on the leeward side of the profile, measured very close to the leading edge, decreases with increase in the local angle of attack until incipient flow separation;
ii. When stall occurs, the leading edge leeward pressure increases;
iii. The amplitude of the suction peak after reattachment increases with increasing angle of attack but decreases when the trailing edge separation point moves a long way forward.

It should be remarked that the pathlines have not been measured but are not necessary horizontal. Hence, the angle of attack at the leading edge is not in the horizontal plane. The pressure is measured in a body fixed sense and measured sections are roughly

horizontal when the model is upright but are inclined when the model is heeled.

The following observations can be drawn from the pressure trends shown in Figure 5. On the lowest sections (first and second plot from the bottom) the leading edge suction decreases with increasing heel, and the trailing edge separation occurs later at 10° heel than at 0° heel. Both these observations may be due to a smaller angle of attack. The sail shape does not change with the heel angle but, considering horizontal sections parallel to the floor, the geometry rotation of the sail causes the camber of the lowest horizontal sections to increase and the camber of the highest horizontal sections to decrease. The flying shape of the A2 sailing at 55° AWA has been detected with a photogrammetric technique. The camber measured on the horizontal section at the clew height increases by roughly 10% when heeled to 10°, and by 20% when heeled to 20°. Increasing the camber causes the suction peak after reattachment to increase. This can explain the earlier separation of the lowest section at 20° heel. On the highest sections (uppermost plot), when the heel angle is increased the camber decreases but the flow is already fully separated and hence is insensitive to this.

Different interpretations of the pressure trends shown in Figure 5 are possible and further investigations are necessary to understand completely what is happening. Interestingly, the present results show that the heel effect is far from being a simple reduction of the effective apparent wind angle and effective apparent wind speed, whose definitions are reported in [19], and is also far from being related only to the edge separation at the shear line of the deck [20]. Wind-tunnel force measurements have been performed by [21], [22] and [23] on upwind sails to investigate the heel effect. These authors reported a reduction of the drive and side forces with heel. More recently, forces have been measured in downwind conditions [24] and a force increase at low heel angles was reported. The present pressure measurements show that the drive force increase at low heel angles is correlated with a larger suction peak, whilst the drive force decrease at large heel angles is correlated with an earlier trailing edge separation.

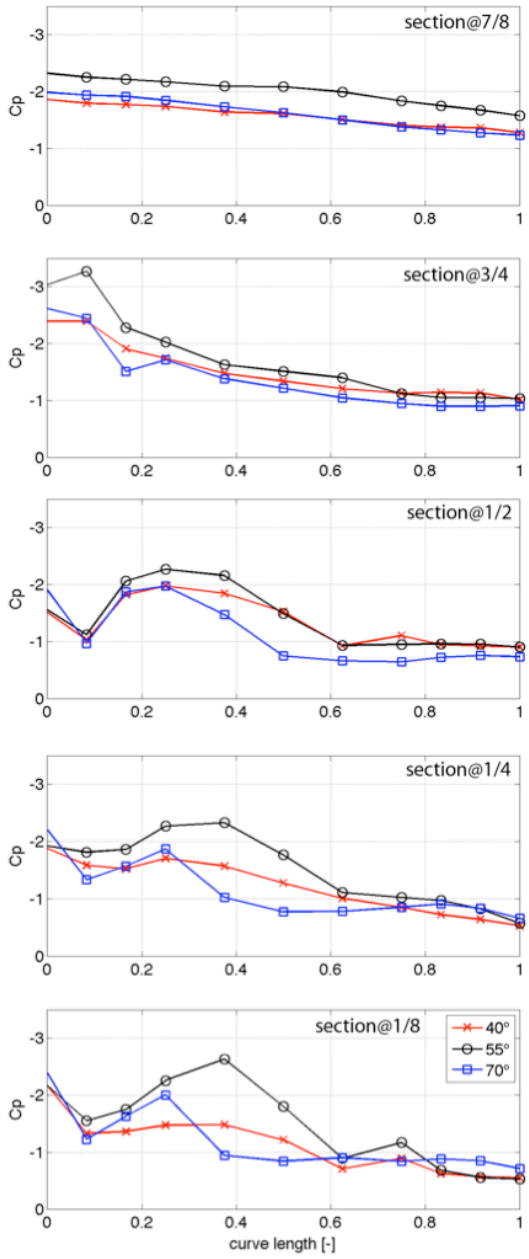

Figure 4: Cp versus the curve length for 40°, 55° and 70° AWA, measured at the different fractions of the mitre (from the top to the bottom): 7/8, 3/4, 1/2, 1/4, 1/8, respectively.

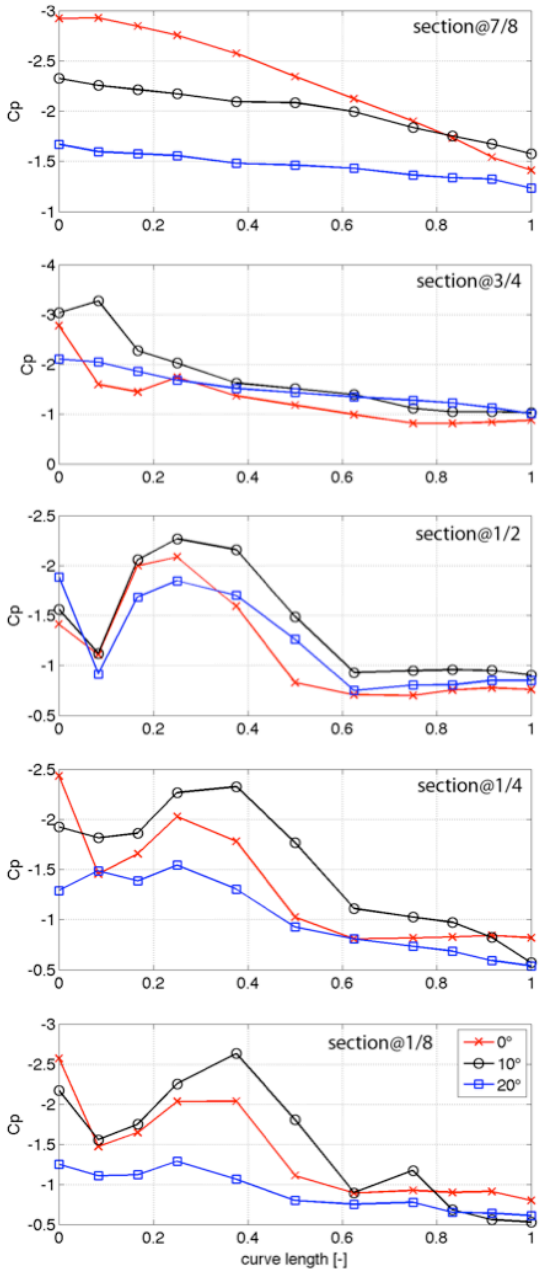

Figure 5: Cp at 55° AWA versus the curve length for 0°, 10° and 20° heel, measured at different fractions of the mitre (from the top to the bottom): 7/8, 3/4, 1/2, 1/4, 1/8, respectively.

4.3 EFFECT OF SAIL SHAPE

The 3 sails had different shapes and were designed for different purposes. As noted above, the A1 is designed to sail at low AWAs and the A3 is designed for large AWAs. The A2 is an all purpose sail which can be sailed at medium AWAs with good performance but has a wider AWA range where the performance is still acceptable even if not optimum. The force trends show that the A1 performs better than the other sails at low AWAs and that the drive force does not decrease with increased heel. Conversely, the A3 performs better at higher AWAs but drive force quickly decreases with increased heel. The A2 shows an intermediate behaviour. These trends are confirmed by the pressure measurements showing that the main force differences are related to the different pressure distributions on the leeward side of the spinnaker. As an example, the pressure measured at the mid-section of each of the 3 sails is presented in Figures 6, 7 and 8 for AWAs of 40°, 55° and 70°, respectively and 10° heel.

At 40° AWA (Figure 6), the A1 shows a higher leading edge suction peak and a minor pressure recovery, which is correlated to a larger angle of attack due to the lower camber of the horizontal sections of the A1. This allows the A1 to generate the maximum suction peak after a small pressure recovery.

At 55° AWA (Figure 7), the A2 shows the maximum suction peak after the reattachment of the leading edge separation. At the lowest sections (not shown in figure) the difference between the suction of the A2 and suction of the other two sails becomes even larger. The trailing edge separation does not change significantly and is about 60% of the curve length for all the sails.

Finally, at 70° AWA (Figure 8), the A3 shows the maximum suction peak after the reattachment of the leading edge separation. The trailing edge separation point occurs at about 50% of the curve length for both the A3 and A2, and the A3's highest suction peak is related to the largest camber of the sail. At the lowest sections (not shown in figure) the differences between the Cp of the A3 and Cp of the other two sails becomes larger than 0.5.

In conclusion, the A1 takes advantage of a flatter entrance profile which allows a shorter separated region at the leading edge and hence a large suction on the first quarter of the curve length. The A3 takes advantage of the increased camber to maximise the suction, and the A2 is a compromise optimised for mid-range AWAs.

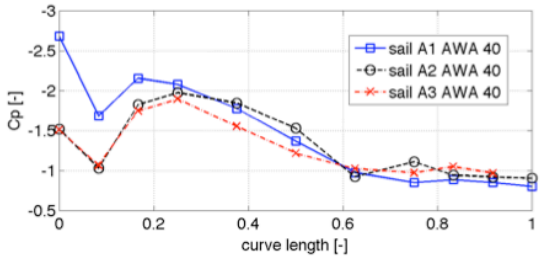

Figure 6: Cp at 40° AWA on the leeward side of the A1, A2 and A3 mid-sections respectively.

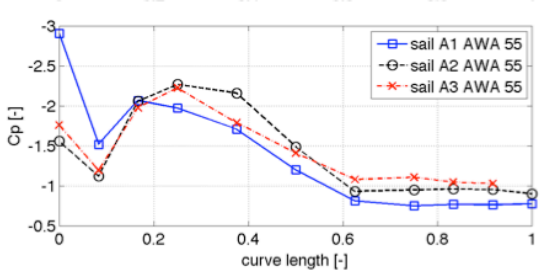

Figure 7: Cp at 55° AWA on the leeward side of the A1, A2 and A3 mid-sections respectively.

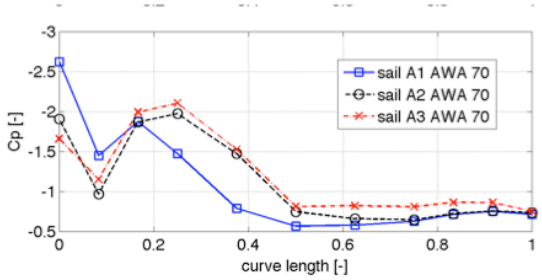

Figure 8: Cp at 70° AWA on the leeward side of the A1, A2 and A3 mid-sections respectively.

4.4 EFFECT OF TWISTED FLOW

The flow was twisted using the vanes shown in Figure 1 to approximately simulate the onset flow that a yacht sailing at a speed of 7 m/s in a true wind speed of 6 m/s at a true wind angle of 140° would experience. The twist profile was kept unchanged for tests discussed in this section. Figure 9 shows the resultant deflection angle of the wind tunnel flow measured at different heights at the model location in the empty test section. The ordinate shows the ratio between the vertical height z and the model height h, the abscissa shows positive values when the flow deflection acts at an increased yaw angle. The twisted flow device changes the angle of attack of the horizontal sections of the sails. Comparing the twisted flow testing condition with the uniform flow testing condition, it is evident that above a height of 0.26h (10m height in full-scale) the higher the section, the more the angle of attack increases. Conversely below 0.26h the lower the section, the more the angle of attack decreases. Note that the deflection angle is defined in the horizontal plane. At the lowest measured point the local AWA is reduced by about 15°. Conversely, at the top of the mast the AWA is increased by about 10°. The deflection of the flow leads also to a deviation angle in the vertical plane. However, the deviation angle has opposite sign on the two sides of the test section and it is negligible in a wide region in the centre of the test section, where the model is located.

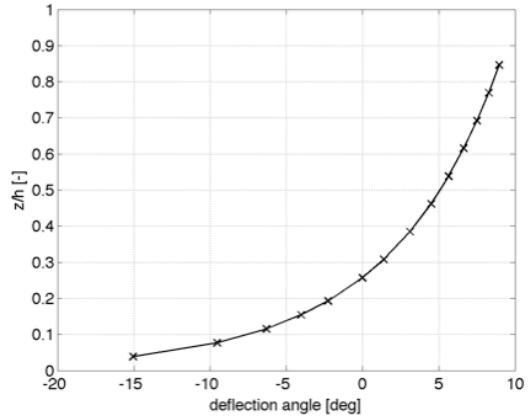

Figure 9: Deflection angle due to the twisted vanes.

Figure 10 shows drive force coefficient Cx achieved by the A3 at 10° heel at the various AWAs when the spinnaker is trimmed to maximise the drive force and when it is trimmed by tightening the sheet just enough to avoid the luff flapping. The two trims were measured both in uniform flow conditions and in twisted flow conditions. Easing the sheet of the A3 enough to let the luff flap leads to the force increasing. Moreover, both of the two trims show a force increase when measured in the twisted flow.

Figure 11 shows the drive force coefficient variation with the heel angle at 55° AWA and the same results are achieved. The drive forces measured with the twisted flow are higher than the forces measured in uniform flow. The force increase due to the twisted flow is larger in the upright condition than in the heeled condition. The twisted flow can increase the drive force by up to 30% when upright but by only 5% at 20° of heel. This is largely due to the angle of attack difference between the lowest and highest sections of the sail, being smaller when the boat is heeled than when it is upright.

The force measurements show that the drive force increases with the increased angle of attack at higher sections and decreases at lower sections due to the twisted flow. This is not unexpected as it is designed to sail in the apparent wind which is twisted when sailing a real yacht in a breeze.

The pressure measurements allow an investigation of how the pressure on the low and high sections change if tested in uniform flow or in twisted flow.

Figure 12 shows the pressure measured on three horizontal sections of the A3 at 55° AWA and 10° heel, both with and without the twisted flow. The sections are measured at ¾, ½ and ¼ of the sail, from top to bottom in the figure, respectively. The pressure distribution measured on the leeward side of the sail with the twisted flow shows higher suctions both on the highest sections and on the lowest sections. The suction increase at the highest section was expected because of the positive flow deflection due to the onset twisted flow. However, the suction increased at the lowest section even though the twisted flow causes a negative flow deflection. Hence a significant 3-dimensional flow effect must occur.

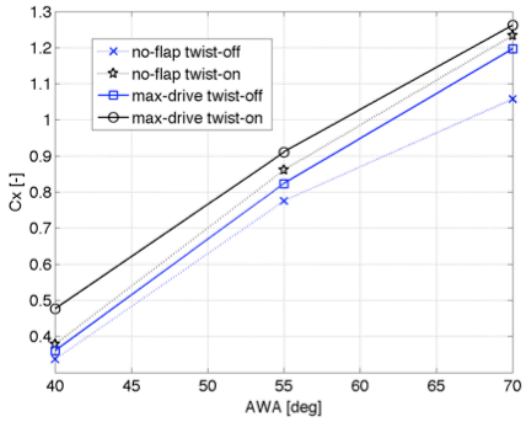

Figure 10: Cx versus the AWA with and without twisted flow for the A3 at 10° heel.

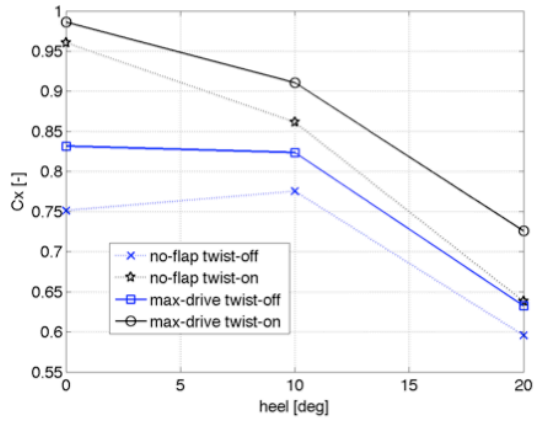

Figure 11: Cx versus the heel angle with and without twisted flow for the A3 at 55° AWA.

One open question for further investigation is if a twist reduction of the sail would also increase the drive force. In fact, by decreasing the twist of the sail, or by introducing the twisted flow, a smaller angle of attack on the highest sections compared to the lowest is achieved.

It should be noted that the twisted flow can increase the drive force of each sail slightly differently, and consequently it affects the crossover between the sails. For this reason when sail crossovers have to be investigated, the twisted flow device should be used.

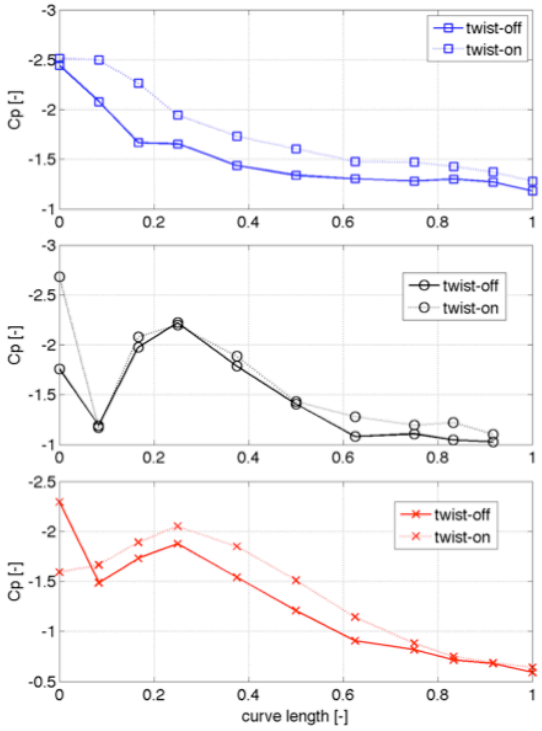

Figure 12: Cp with and without twisted flow versus the curve length, measured at 3/4, 1/2, 1/4 of the mitre (from top to bottom), respectively, for A3 at 55° AWA and 10° heel.

5. CONCLUSIONS

Experimental tests were performed on a 1/15th scale model in the Yacht Research Unit's Twisted Flow Wind Tunnel in preparation for Emirates Team New Zealand's challenge for the 33rd America's Cup. Three off-wind sails, named A1, A2 and A3 respectively, were tested with the same mainsail at apparent wind angles of 40°, 55° and 70° and at heel angles of 0°, 10° and 20° and their pressure distributions measured. These pressure measurements showed that the measured force trends are clearly correlated with the pressure distribution on the leeward side of the asymmetric spinnaker.

In particular the pressure distribution results enable the following conclusions to be drawn.

1. The sail's trim changes significantly when the apparent wind angle increases, which leads to a

different sail shape and different angle of attack. When larger AWAs are sailed, the spinnaker sheet is eased, which increases the camber and decreases the angle of attack. But the combination of the increase in apparent wind angle and the sheet ease is still an increased angle of attack. The pressure measurements show that, in the first stage, increasing the apparent wind angle causes the suction to increase. Then, when the apparent wind angle is further increased, the suction cannot increase anymore because the higher adverse pressure gradient causes trailing edge separation to occur first.

2. Some asymmetric spinnakers (e.g. the A2) show the maximum drive force when slightly heeled. The pressure distribution on the leeward side of the A2 shows that the drive force increase at low heel angles is correlated with a larger suction peak, whilst the drive force decrease at large heel angles is correlated with an earlier trailing edge separation.

3. The 3 sails showed good correlation between their design purpose and the measured pressures. The pressure measurements gave an explanation of the force trends, allowing a deeper understanding of the sail's characteristics. In particular the A1, which is designed for close apparent wind angles, shows a high suction on the forward region, due to a small camber. This projects the aerodynamic force forward, which is necessary when sailing at close angles. On the contrary, when sailing at deeper angles the A1 shows a larger trailing edge separation, which compromises its performance, while in the same sailing condition the A3 shows the maximum suction due to its larger camber. The A2 pressure distribution doesn't change significantly when the apparent wind angle is increased, and it achieves the maximum suction at 55° apparent wind angle, which confirms the A2's all-purpose design.

4. Finally, the effect of the twist on the force and pressure measurements was investigated. The same tests were performed with and without twisted flow onto the yacht model. The twisted flow decreases the angle of attack onto the lower sections and increases it onto the highest sections of the sail. All the tests performed at the 3 apparent wind angles and at the 3 heel angles showed a force increase when the twisted flow was used. The pressure measurements showed that the suction on the leeward side of the spinnaker increased both on the lowest and highest sections, which suggests the existence of dominant and important 3D aerodynamic effects that are incorrectly modelled in uniform flow.

6. ACKNOWLEDGMENTS

The authors would like to thank Frederik Gerhardt for his enthusiasm in providing new ideas und suggestions for the research. The support of the YRU, especially David Le Pelley and Nick Velychko is gratefully acknowledged.

7. REFERENCES

1. VIOLA I.M. AND FLAY R.G.J., Force and Pressure Investigation of Modern Asymmetric Spinnakers, *International Journal of Small Craft Technology,* Trans. RINA, vol. 151, part B2, pp. 31-40, 2009..
2. MARCHAJ C., Aero-Hydrodynamics of Sailing, *Dodd Mead and Company, New York,* 1979.
3. GENTRY A., The Aerodynamics of Sail Interaction, *In the proceedings of the 3rd AIAA Symposium on the Aero/Hydronautics of Sailing, Redondo Beach, California, November 20th*, 1971.
4. GENTRY A., The Application of Computational Fluid Dynamics to Sails, *In the proceedings of Symposium on Hydrodynamic Performance Enhancement for Marine Applications, Newport, Rhode Island,* October 31st – November 1st, 1988.
5. WILKINSON S., Partially Separated Flows Around 2D Masts and Sails, *PhD Thesis, University of Southampton,* 1984.
6. WILKINSON S., Static Pressure Distribution over 2D Mast/Sail Geometries, *Journal of Marine Technology, Volume 26, (4), pp* 333–337, October 1989.
7. WILKINSON S., Boundary–Layer Explorations Over a Two–Dimensional Mast/Sail Geometry, *Journal of Marine Technology, Volume 27, pp 250-256,* 1990.
8. CHAPIN V.G., JAMME S., CHASSAING P., Viscous Computational Fluid Dynamics as a Relevant Decision-Making Tool for Mast-Sail Aerodynamics Downwind Sail Aerodynamics: a CFD Investigation with High Grid Resolution, *Journal of Marine Technology, Volume 42, 1, pp 1-10,* January 2005.
9. ABBOT IH & VON DOENHOFF AE., Theory of Wing Section. *Dover Publications Inc, New York. ISBN: 0-486-60586-8,* 1949.
10. CROMPTON MJ & BARRET RV. Investigation of the separation bubble formed behind the sharp leading edge of a flat plate at incidence. *Proceedings of the Institution of Mechanical Engineers, Part G: Journal of Aerospace Engineering (ISSN 0954-4100), Volume 214, (3), pp 157-176,* 2000.
11. THWAITES B. Incompressible Aerodynamics. *Dover Publications Inc, New York. ISBN: 0-486-65465-6,* 1969.
12. COLLIE S., GERRITSEN M., The Challenging Turbulent Flows Past Downwind Yacht Sails and Practical Application of CFD to Them, *In the proceeding of the 2nd High Performance Yacht Design Conference (HPYDC2), Auckland, New Zealand, pp 30-41,* February 13th-16th, 2006.
13. FLAY R.G.J., MILLAR S., Experimental Consideration Concerning Measurements in Sails: Wind Tunnel and Full Scale, *In the proceedings of the 2nd High Performance Yacht Design*

Conference (HPYDC2), Auckland, New Zealand, February 14th-16th, 2006.

14. PUDDU P, ERRIU N, NURZIA F, PISTIDDA A, MURA A: Full Scale Investigation of One-Design Class Catamaran Sails, *In the proceeding of the 2nd High Performance Yacht Design Conference (HPYDC2), Auckland, New Zealand,* February 14th-16th, 2006.
15. GAVES W, BARBERA T, BRAUN JB, IMAS L: Measurements and Simulation of Pressure Distribution on Full size scales, In the proceeding of the 3rd *High Performance Yacht Design Conference (HPYDC3), Auckland, New Zealand,* December 2nd-4th, 2008.
16. RICHARDS P.J. & LASHER W.C., Wind Tunnel and CFD Modelling of Pressures on Downwind Sails, *In proceedings of the 6th International Colloquium on Bluff Bodies Aerodynamics & Applications (BBAAVI), Milan, Italy,* July 20th-24th, 2008.
17. FLAY R.G.J., A Twisted Flow Wind Tunnel for Testing Yacht Sails, *Journal of Wind Engineering and Industrial Aerodynamics, Volume 63, pp. 171-182,* 1996.
18. GERHARDT F., Investigation of Time Averaged and Fluctuating Velocity Components in The Wake of Twisting Vanes, *BE thesis, Lehrstuhl und Institut fuer Allgemeine Konstruktionstechnik des Maschinenbaus, RWTH-Aachen, Aachen, Germany,* January 2005.
19. KERWIN J.E., A Velocity Prediction Program for Ocean Racing Yachts revised to February 1978, *Report No. 78-11, Massachusetts Institute of Technology, Boston, USA,* 1978.
20. HANSEN H., Enhanced Wind Tunnel Techniques and Aerodynamic Force Modelling for Yacht Sail, *PhD Thesis, Yacht Research Unit, Mechanical Engineering Department, The University of Auckland, New Zealand,* July 18th, 2007.
21. JACKSON P.S., Modelling the Aerodynamics of Upwind Sails, *Journal of Wind Engineering and Industrial Aerodynamics, Volume 63, pp 17-34,* 1996
22. DEAKIN B., Model Test Techniques Developped to investigate the Wind Heeling Characteristics od Sailing Vessels and Their Response to Gusts, *In the proceedings of the 10th Chesapeake Sailing Yacht Symposium, pp. 83-93, February 9th,* 1991.
23. CAMPBELL I.M.C., Optimization of a Sailing Rig using Wind Tunnel Data, *In the proceedings of the 13th Chesapeake Sailing Yacht Symposium, pp. 49-63, January 25th,* 1997.

24. Le PELLEY D., EKBLOM P., FLAY R.G.J., Wind Tunnel Testing of Downwind Sails, *In the proceedings of the High Performance Yacht Design Conference (HPYDC), Auckland, New Zealand, December 2nd-6th,* 2002.